

Volume 2, Issue 1, Jan.- June 2025

ISSN (Print): 3049 - 2548 ISSN (Online): 3049 - 0146

RESEARCH ARTICLE

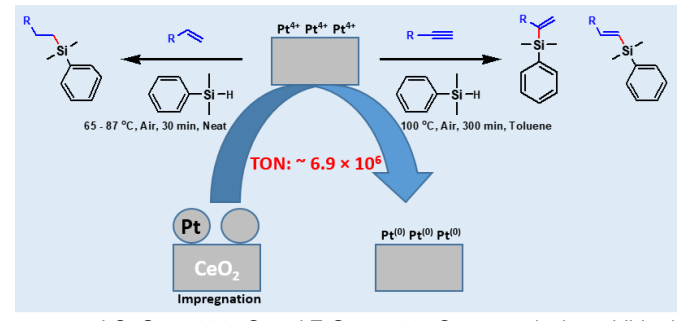
Rational Design of Pt Supported Catalysts for Hydrosilylation: **Influence of Support and Calcination Temperature**

Kazu Okumura a* D, Shinsaku Aikawaa, Yuki Aokia, Anas Abdullahia, and Mustapha G. Mohammedb

a Department of Applied Chemistry, School of Advanced Engineering, Kogakuin University, 2665-1 Nakano-machi Hachioji-city, 192-0015, Tokyo, Japan. Department of Chemical Engineering, Faculty of Engineering, Universiti Malaya, 50603, Kuala Lumpur, Malaysia *Correspondence: okmr@cc.kogakuin.ac.jp (K. Okumura)

Abstract: The hydrosilylation reaction plays a significant role in organosilicon chemistry, enabling the formation of silicon-carbon bonds crucial for industrial and specialty chemical production. While homogeneous platinum catalysts are incredibly efficient, they come with

drawbacks like limited recyclability and high Pt consumption, necessitating researchers to develop more durable, heterogeneous alternatives. By harnessing the synergies of support materials and thermal treatment, this study aims to develop highly active heterogeneous platinum-supported catalysts for the hydrosilylation reaction. We synthesized Pt-supported catalysts on nine different metal oxide supports using impregnation and heat treatment at 500 -1000 °C. Among them, Pt/CeO₂ 900H, prepared by calcining Pt-supported CeO₂ at 900 °C, followed by reducing it with hydrogen at 500 °C, emerged as the most effective catalyst for alkene hydrosilylation, achieving a turnover number (TON) of 6.9 x 106, comparable to the widely used Karstedt catalyst. For alkyne hydrosilylation, Pt/CeO2 600C and Pt/ZrO2 500C demonstrated



outstanding performance. These catalysts, prepared by calcining Pt-impregnated CeO2 at 600 °C and ZrO2 at 500 °C, respectively, exhibited remarkable activity and stability, maintaining high performance over 10 reaction cycles. These findings highlight how the right combination of support material and thermal treatment can fine-tune Pt catalysts for more sustainable hydrosilylation processes. By providing a scalable and cost-effective alternative to traditional homogeneous catalysts, this work connects fundamental research with industrial applications, advancing greener and more efficient approaches to organosilicon synthesis.

Keywords: Hydrosilylation, alkene, alkyne, platinum catalyst, cerium oxide

Introduction

The hydrosilylation reaction, a key hydrometallation process, is pivotal in the silicone industry. This reaction entails the addition of hydrosilane compounds H_nSiR_{4-n}, (where n = 1 or 2, and R = alkyl, aryl, or alkoxy groups) to unsaturated hydrocarbons such as olefins, dienes, and acetylenes, resulting in the formation of alkyl silanes.1 The origins of modern hydrosilylation chemistry trace back to 1947, when Sommer published his groundbreaking report on the trichlorosilane addition to 1-octene catalyzed by peroxide, established a foundational milestone for subsequent advancements in the field.2 Since then, hydrosilylation has evolved into a cornerstone of organosilicon chemistry, with its industrial and academic significance driving continuous innovation in catalyst design and reaction optimization. The profound significance of this reaction stems from its ability to efficiently construct silicon-carbon bonds, which are fundamental to the properties of numerous industrial materials.3

Beyond its indispensable role in the silicone industry, hydrosilylation finds extensive application in the synthesis of fine chemicals.4 Its remarkable versatility is highlighted by its ability to proceed efficiently even in the existence of sensitive functional groups like epoxides. This property is valuable in a variety of applications, ranging from the formulation of siliconcontaining paints to the precise functionalization of polymers unsaturated bonds. For dimethylpolysiloxane, a ubiquitous silicone rubber, can be tailored through cross-linking with vinyl silicone reagents, demonstrating the reaction's capacity to impart specific properties to polymeric materials.

Transition metals from group 9 and 10, particularly platinum-based catalysts like the Speier catalyst (H2PtCl6) and Karstedt catalyst (O[Si(CH₃)₂CH=CH₂]₂Pt), are highly effective for hydrosilylation. These homogeneous catalysts achieve remarkable efficiency, often requiring as little as 0.1

mol% Pt. However, their recovery and reuse remain challenging, leading to significant Pt consumption with approximately 5.6 tons of Pt used in the organosilicon industry. This has spurred efforts to develop heterogeneous catalysts that can be recycled to reduce Pt usage. Additionally, research has explored cheaper and more abundant transition metals (Co⁵, Fe⁶, etc.) based catalysts, though these have yet to find industrial application.7

Nevertheless, the unparalleled catalytic activity of platinum-based systems continues to anchor industrial hydrosilylation processes.⁸ Among these, Karstedt's catalyst remains the most widely used and versatile, acting as the benchmark for assessing new catalyst. The mechanistic intricacies of hydrosilylation over homogeneous catalysts have been meticulously dissected, revealing two primary pathways: the Chalk-Harrod mechanism and its improved variant. Both pathways initiate with oxidative addition to the metal center. However, they diverge in the subsequent steps. The Chalk-Harrod mechanism posits hydride insertion and subsequent reductive elimination as the rate-determining step, while the modified mechanism favors silyl insertion, followed by isomerization to form Z-alkenyl silanes, thereby mitigating steric repulsion. This modified mechanism better explains the behaviors of Ru, Rh, and Ir catalyzed systems.9 Despite their undeniable efficacy and mechanistic insights, the drawbacks of homogeneous catalysts, including limited recyclability and sensitivity to reaction conditions, have spurred the development of robust, heterogeneous alternatives.10

Recent advancements in heterogeneous catalysis have opened new avenues for addressing these challenges. Supported platinum catalysts, in particular, have emerged as offering promising alternatives, enhanced recyclability, and tunable activity through rational design of the support material and optimization of catalyst preparation parameters. 11 The selection of support materials, ranging from metal oxides (e.g., Al₂O₃, SiO₂) to carbon-based substrates, is crucial in tailoring the electronic and geometric properties of Pt nanoparticles, directly impacting their catalytic performance. ¹² Furthermore, calcination temperature critically influences dispersion, oxidation state, and stability of Pt species, which are essential for maximizing activity and selectivity in hydrosilylation. ¹³

The influence of these electronic and geometric properties can be found in literature. For instance, single-site Pt catalysts supported on Al₂O₃ or TiO₂ have demonstrated remarkable activity in hydrosilylation reactions. 14 Beller et al. reported that Pt/NR-Al₂O₃-IP, prepared by impregnating alumina nanorods with H2PtCl6 · H2O, achieved six reuse cycles and a maximum turnover number (TON) of 300,000 even in the presence of highly reactive functional groups. 15 Similarly, Wang et al. developed a single-site Pt catalyst $(Pt^{\delta+}/TiO_2)$ using electrostatic induced ion exchange and a two-dimensional confinement strategy. This catalyst was successfully reused five times, with density functional theory (DFT) calculations attributing its high activity to the atomic dispersion of the active species and the electronic structure of the partially positively charged Pto+, which is not present in conventional nanocatalysts.16

In another study, Gupton *et al.* utilized solvent-free microwave irradiation of graphene loaded with Pt as a precursor of $PtCl_4^{-2}$ which leads to the reduction of $PtCl_4^{-1}$ and the formation of graphene defects or holes that strongly anchor Pt nanoparticles. The resulting catalyst exhibited turnover frequency (TOF) of 4.8×10^6 h⁻¹ and a TON of 9.4×10^6 , enabling continuous hydrosilylation in a packed-bed reactor.¹⁷

In our laboratory, we reported that Pt supported on MgO and heat-treated at high temperature can control Pt dispersion through solid solution formation and re-deposition, suggesting that the behavior of Pt changes with thermal treatment and serves as the foundation for further optimization.

18 Building on these insights, this study explores the hydrosilylation of alkenes and alkynes using Pt catalysts supported on various oxides and subjected to high-temperature treatments. The highly active catalysts are characterized through advanced techniques such as X-ray absorption fine structure (XAFS) spectroscopy, and their reusability is assessed in alkyne hydrosilylation. This work seeks to advance the design of efficient and recoverable heterogeneous catalysts for sustainable hydrosilylation processes.

This study marks a significant advancement toward sustainable and efficient catalytic systems, effectively bridging fundamental research with industrial application. By overcoming the limitations of existing catalysts and presenting a scalable, cost-effective alternative, our approach holds the potential to transform organosilicon compound synthesis, fostering greener and more efficient chemical processes.

The catalysts are designated as Pt/Support xC or Pt/Support xH, where x represents the calcination temperature in degrees Celsius, C and H represent pre- and post-reduction, respectively. For example, platinum supported on Al_2O_3 , calcined at 500 °C and reduced is labeled as Pt/Al $_2\text{O}_3$ 500H.

Results and Discussion

Reactions using alkenes as substrates

To study the effect of support and thermal treatment temperature on the hydrosilylation reaction using alkenes as the substrates, the reaction was conducted using Pt supported on nine different metal oxides and calcined at different temperatures (500 - 1000 $^{\circ}\text{C}).$ Figure 1(a) and (b) illustrate the relationship between heat treatment temperature

and reaction yield for Pt catalysts supported on different metal oxides, comparing those subjected to heat treatment alone and those further reduced, respectively. Among the pre-reduced catalysts, Pt/ZrO₂ 700C exhibited the highest activity. At higher temperatures, Pt/MgO and Pt/CeO₂ also demonstrated significant activity, with the yield of Pt/CeO₂ progressively increasing as the calcination temperature rose.

Notably, catalysts that underwent reduction generally exhibited enhanced activity compared to their heat-treated counterparts, with Pt/CeO₂ 900H displaying the highest performance (Figure 1(b)). At lower temperatures, Pt/ZrO₂ 500H and Pt/TiO₂ 500H also showed considerable activity; however, their performance declined upon heat treatment at higher temperatures. In contrast, catalysts supported on CeO₂ exhibited improved activity with increasing temperature.

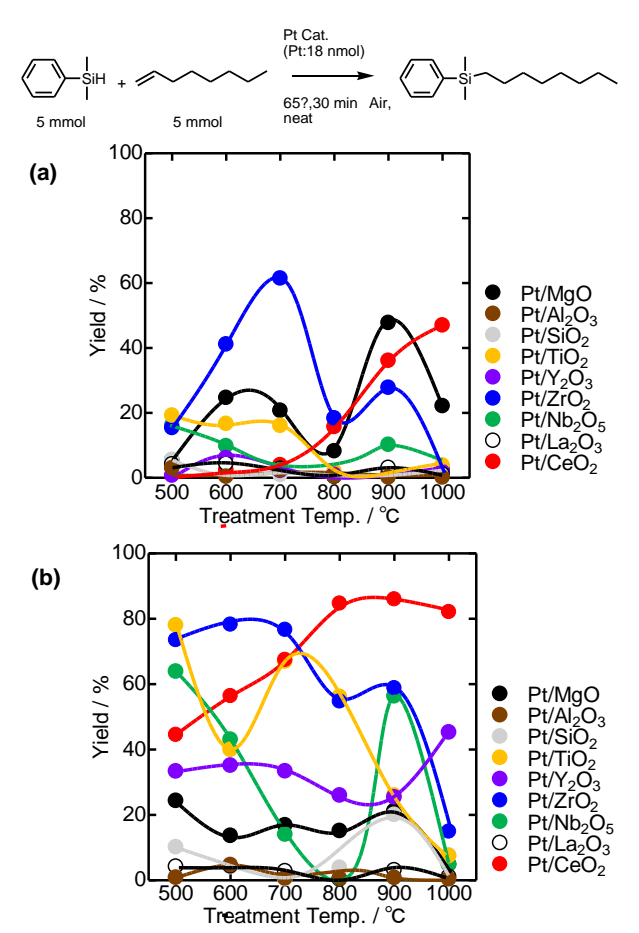


Figure 1. (a) The relationship between thermal treatment temperature and yield in the reaction of alkenes with catalysts prior to reduction treatment. (b) The relationship between thermal treatment temperature and yield in the reaction of alkenes with catalysts after the reduction treatment with hydrogen.

Figure S1 (a) shows the change over time of the reaction catalyzed by Pt/CeO2 900H at 47 and 65 °C. The vield obtained after 2 h at 47 °C was 80%, while the yield obtained after 1 h at 65 °C reached 92%. Next, the reaction was performed at 65 °C using Pt/CeO₂ 500H-1000H. The highest activity was obtained with Pt/CeO2 800H and 900H; the yield reached over 90% in 1 h using these catalysts (Figure S1(b)). indicate that the hydrosilylation of dimethylphenylsilane with 1-octene should be performed at 65 °C for 1 h to obtain yields higher than 90% using Pt/CeO₂ 800H or 900H catalysts. The catalytic performance of Pt/CeO₂ 900H was particularly interesting because the activity of metal-supported catalysts usually decreases with increasing temperature as the particle size increases, which not only reduces the number of accessible atoms for adsorption but also reduces the surface energy of the atoms due to the coordination effects.

Table 1. Influence of Pt precursors on the reaction in Pt/CeO2

Catalyst	Time (h)	Yield (%)	TON
Ptnp/CeO ₂ 900H	1	85	2.4×10 ⁵
Pt(acac) ₂ /CeO ₂ 900H	1	78	2.2×10 ⁵

To assess the impact of the Pt precursor on catalytic activity, $Pt(acac)_2/CeO_2$ 900H was prepared using $Pt(acac)_2$ as the precursor and compared with $Ptnp/CeO_2$ 900H, which was synthesized using a Pt nanoparticle solution (Table 1). Time-course change in the yield over time is shown in Figure S2. When $Pt(acac)_2$ was used as the precursor, the reaction yield decreased by approximately 8% at 60 min, and the turnover number (TON) declined by about 2×10^4 . However, no significant overall changes were observed, suggesting that the choice of Pt precursor had a limited impact on the catalytic performance of Pt/CeO_2 .

To investigate the potential role of basic sites on CeO_2 in the catalytic reaction over Pt/CeO_2 , catalytic tests were conducted under different gas circulation conditions following heat treatment and reduction. Allylbenzene was used as the alkene substrate, with the results summarized in Table 2. The overall variations in activity were minimal. Notably, the yield remained largely unchanged even after O_2 distribution, indicating that air oxidation of the reduced catalyst had little to no impact on its catalytic performance. These findings suggest that the reaction atmosphere does not significantly influence the reaction.

Table 2. Effect of gas reaction atmosphere on the reaction for Pt/CeO₂ 900H

Catalyst	Flow gas	Yield (%)	TON
Pt/CeO ₂ 900H	None (air)	87	2.2×10⁵
Pt/CeO ₂ 900H	N_2	82	2.2×10 ⁵
Pt/CeO ₂ 900H	O_2	86	2.4×10 ⁵
Pt/CeO ₂ 900H	CO_2	85	2.3×10⁵

To investigate the effect of temperature on the reaction during the reduction process following heat treatment, experiments were carried out using Pt/CeO $_2$ 900H catalysts reduced at varying temperatures. Allylbenzene was used as the alkene substrate, and the results are presented in Table 3. High catalytic activity was observed at reduction temperatures above 200 °C, with no significant change in activity between 200 °C and 700 °C.

However, at 600 °C and 700 °C, a decline in yield was noted after the reaction. Based on these findings, a reduction temperature of 500 °C was selected to maintain consistency across different catalyst supports. To assess the dispersion of Pt in the prepared catalysts, CO chemisorption measurements were performed. Figure 2 illustrates the relationship between heat treatment temperature and dispersion of Pt on the various supports, revealing a bimodal distribution for MgO, Y_2O_3 , and La_2O_3 , with distinct peaks at

ca. 600 and 900 °C. The dispersion can be correlated with the electronegativity of support cations, as discussed in the reference.¹⁸

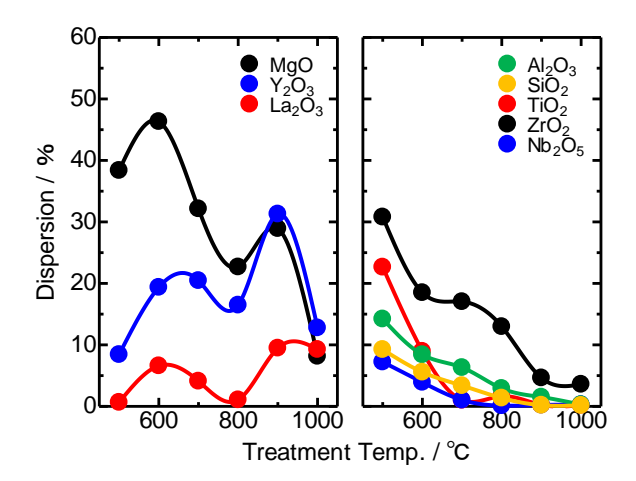


Figure 2. Relationship between heat treatment temperature and dispersion of Pt on various supports measured with CO adsorption.

Table 3. Effect of reduction temperature on reaction for Pt/CeO₂

Catalyst	Reduction Temp. (°C)	Yield (%)	TON
Pt/CeO ₂ 900H	100	22	6.0×10 ⁴
Pt/CeO ₂ 900H	200	75	2.1×10 ⁵
Pt/CeO ₂ 900H	300	82	2.3×10 ⁵
Pt/CeO ₂ 900H	400	81	2.4×10 ⁵
Pt/CeO ₂ 900H	500	85	2.2×10 ⁵
Pt/CeO ₂ 900H	600	72	2.3×10 ⁵
Pt/CeO ₂ 900H	700	79	2.1×10 ⁵

STEM-HAADF imaging and EDS mapping were performed to investigate the dispersion and distribution of Pt in highly active Pt/CeO₂ catalysts. In Pt/CeO₂ 500C (Figure S3), Pt particles were observed in the EDS mapping, whereas no distinct Pt particles were detected in Pt/CeO₂ heat-treated above 600 °C using STEM-HAADF (Figure S4). Figure S5(a) and (b) present the STEM-HAADF images of Pt/CeO₂ 900C and Pt /CeO₂ 900H, respectively, revealing that no Pt particles were observable before reduction treatment (Pt/CeO₂ 900C); however, after reduction treatment (Pt/CeO₂ 900H), finely dispersed Pt particles were deposited as observed in the EDS mapping (Figure S5(c)). These Pt particles are considered to contribute significantly to the high catalytic activity observed in the reaction.

Figure S6 illustrates the relationship between reduction temperature, lattice distortion and crystallite size of Pt/CeO₂ 900H, as determined by temperature-programmed XRD measurements. The analysis was conducted at temperatures of 100, 200, 300, 400, 500, 700, and 900 °C, starting from room temperature and finally cooling back to room temperature. The CeO₂(111) diffraction peak was used to calculate lattice distortion and crystallite size. Lattice distortion increased from room temperature to 300 °C before subsequently decreased, whereas the crystallite size remained relatively unchanged up to 500 °C but exhibited a significant increase at higher temperatures. These findings suggest that up to 300 °C, Pt remains in a solid solution or is surface-dispersed, resulting in a structurally disordered state with high strain. However, at higher temperatures, the structure becomes well-defined, with reduced strain and increased crystallite size, likely due to thermal effect.

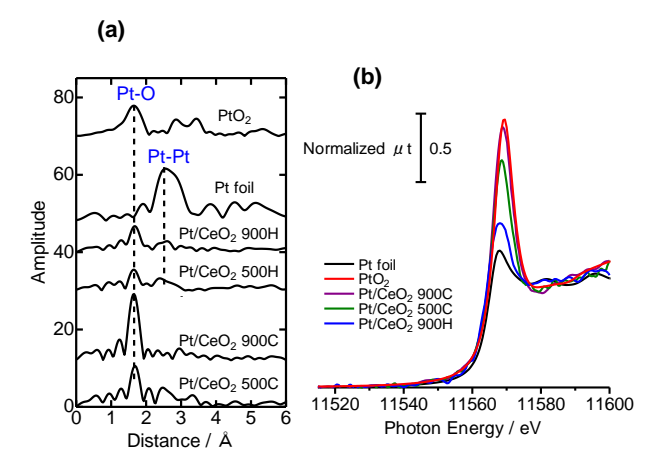


Figure 3. Pt L₃-edge (a) EXAFS radial distribution function and (b) XANES of Pt/CeO₂.

Figure 3(a) and (b) presents Pt L_3 -edge EXAFS and XANES spectra for Pt/CeO₂ 500C, Pt/CeO₂ 900C, and Pt/CeO₂ 900H, together with reference ones, respectively. In Pt/CeO₂ 900C, the EXAFS spectra in Figure 3(a) are dominated by Pt–O interactions, with almost no Pt–Pt interactions, indicating a high dispersion of Pt in the oxidized state. In contrast, Pt/CeO₂ 500H and Pt/CeO₂ 900H exhibit reduced Pt–O signals compared to their pre-reduction states, along with the appearance of a Pt–Pt peak, confirming the presence of Pt(0) in Pt/CeO₂ 900H. This suggests that Pt, initially well-dispersed during high-temperature heat treatment, precipitates as metallic Pt(0) on the surface following reduction. The formation of Pd(0) in Pt/CeO2 500H and Pt/CeO2 900H is consistent with the reduced white line intensity at 11568 eV in XANES (Figure 3(b)).

Figure 4 illustrates in situ CO adsorption FT-IR spectra of Pt/CeO2, the plot represents the difference between spectra measured before and after CO adsorption. Peaks at 2070 and 1600 - 1000 cm⁻¹ are attributed to CO adsorption, with the 2070 cm⁻¹ peak specifically assigned to CO adsorbed on Pt(0). The intensity of CO adsorption peaks is relatively low at heat treatment temperatures of 500 to 700 °C but increases significantly at 800 to 1000 °C. These trends correlate with the yield of alkyne hydrosilylation reactions using Pt/CeO2 after reduction treatment, as shown in Figure 1(b). The increase in the yield in parallel with the higher CO peak intensity at calcination temperatures 800 - 1000 °C suggests that temperatures above 800 °C facilitate the formation of Pt(0) species upon reduction, leading to a higher number of active sites and thereby increasing the reaction vields.

Table 4 and 5 summarizes the results of reactions using various alkenes and hydrosilanes catalyzed by Pt/CeO_2

900H, respectively. Notably, all reactions exhibited TON of 5.3×10⁴ (Table 5, entry 5) or higher, demonstrating the effectiveness of the catalyst across diverse substrates. To further evaluate the catalytic efficiency of Pt/CeO₂ 900H, its performance was compared with that of the industrially used homogeneous Karstedt catalyst. The substrate and reaction conditions are presented in Table 6, where Pt/CeO₂ 900H exhibited high activity almost comparable to the

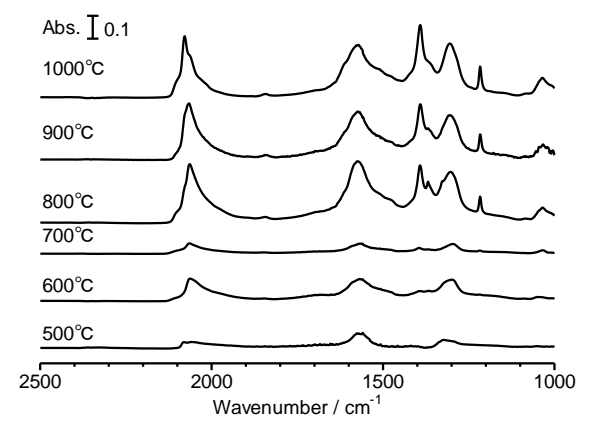


Figure 4. In situ FT-IR spectra of adsorbed CO on Pt/CeO₂.

homogeneous system, underscoring its industrial potential. The plausible mechanism for the high activity of Pt/CeO_2 in the reaction using alkenes as substrates is illustrated in Figure 5, inferred from STEM-HAADF and XAFS analyses. The high activity of Pt on CeO_2 is attributed to the dispersion of Pt on the surface during high temperature heat treatment, followed by its dissolution into the substrate. Subsequent hydrogen reduction treatment leads to the re-deposition of Pt as finely dispersed particles on the surface. This reversible redispersion and deposition process likely contributed to the sustained high activity of the Pt/CeO_2 catalyst.

Table 4. Reaction scope of the Pt/CeO₂ catalyst with various alkenes
Pt/CeO₂ 900H

PhMe ₂ SiH	+	P	t/CeO ₂ 9	00H	DhMo	C:-
1a 5 mmol	2b-2g 5 mmol		Air,neat		PhMe ₂	R
Entry	Substrate		Time (h)	T (°C)	Yield (%)	TON (10⁵)
1		∠ 2b)	2	87	92	2.6
2	○ (20	;)	2	108	89	2.5
3	∫°Si, o (20	d)	4	87	99	0.64
4	◇ ◇◇ (2e	·)	2	87	84	2.4

108

87

4

(2g)

96

87

5

6

0.69

2.4

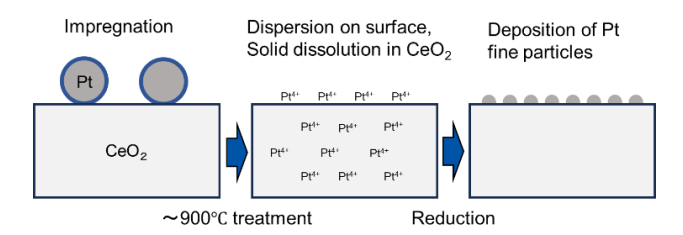


Figure 5. Proposed mechanism of high activity of Pt/CeO₂ in reactions using alkenes as substrates.

Table 5. Reaction scope of the Pt/CeO₂ catalyst with various hydrosilanes

Entry	Substrate	Time (h)	T (°C)	Yield (%)	TON (10 ⁵)
1	PhMe ₂ SiH (1a)	2	87	97	2.8
2	Me(EtO) ₂ SiH (1b)	2	70	91	2.5
3	$HSi(Me)_2OSi(Me)_3$ (1C)	2	87	90	1.6
4	$Si(Me)_3OSiH(Me)_2$ $OSi(Me)_3$ (1d)	4	87	97	0.66
5	(EtO) ₃ SiH (1e)	4	87	81	0.53

Table 6. Comparison with industrially used homogeneous Karstedt catalyst.

Catalyst	Time (h)	Yield (%)	TON
Pt/CeO ₂ 900H	2	62	5.2×10 ⁶
Pt/CeO ₂ 900H	4	71	6.4×10 ⁶
Pt/CeO ₂ 900H	6	77	6.9×10 ⁶
Karstedt Cat.	2	78	7.3×10 ⁶
Karstedt Cat.	4	82	7.7×10 ⁶
Karstedt Cat.	6	85	7.9×10 ⁶

Reactions using alkynes as substrates

Figure 6(a) and (b) illustrate the relationship between heat treatment temperature and reaction yield for Pt catalysts supported on different metal oxides, comparing those subjected to heat treatment alone and those further reduced, respectively. Most Pt-supported oxides exhibited high activity when the catalysts were heat treated at lower temperatures, with a decline in activity observed at higher heat treatment temperatures. However, Pt/CeO₂ catalysts maintained high activity without a significant decrease in yield, even at elevated heat treatment temperatures, particularly in the reactions where the catalyst was reduced with hydrogen prior to the reaction (Figure 6(b)). Since some of the catalysts had yields greater than 90% at 1 h, the catalysts were selected based on yields greater than 40% at 1 h. Figure S7 shows the

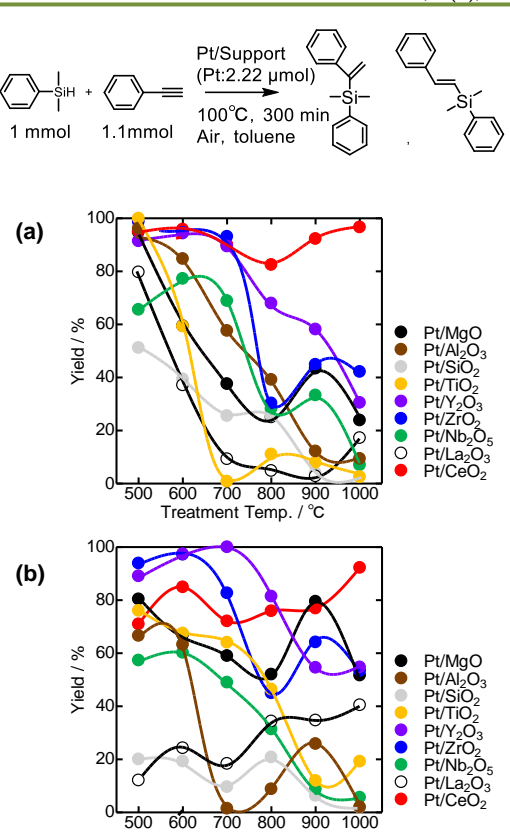


Figure 6. (a) The relationship between thermal treatment temperature and yield in the reaction of the alkyne (phenylacetylene) with catalysts prior to reduction treatment. (b) The relationship between thermal treatment temperature and yield in the reaction of the alkyne (phenylacetylene) with catalysts after the reduction treatment with hydrogen.

Treatment Temp. / °C

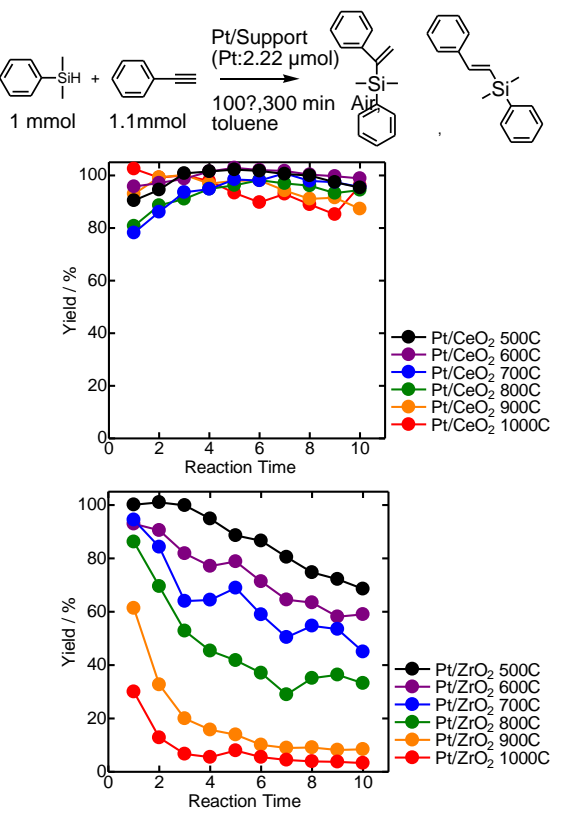


Figure 7. Catalyst reuse in the hydrosilylation of the alkyne (phenylacetylene) with (a) Pt/CeO₂ and (b) Pt/ZrO₂ heat-treated at Various Temperatures.

change of yield over time for each catalyst. Among the tested catalysts, Pt/Al_2O_3 500C, Pt/TiO_2 500C, Pt/Y_2O_3 600C, Pt/Y_2O_3 600H Pt/ZrO_2 500C, and, Pt/CeO_2 600C achieved yields above 40%, with Pt/ZrO_2 500C exhibiting the highest activity.

Figure S8 highlights the recycling performance of highly active catalysts in the hydrosilylation of alkynes. Pt/CeO_2 600C demonstrated exceptional reusability, whereas Pt/ZrO_2 500C and Pt/TiO_2 500C, despite high initial activity, experienced a significant decline in yield after three cycles. The comparative recycling study of Pt/CeO_2 and Pt/ZrO_2 (Figure 7) further confirms that Pt/CeO_2 maintains superior reusability across all heat treatment temperatures. In contrast, the activity and reusability of Pt/ZrO_2 progressively declined with increasing heat treatment temperatures, suggesting that Pt/CeO_2 offers a more robust and durable catalytic system for alkyne hydrosilylation reactions.

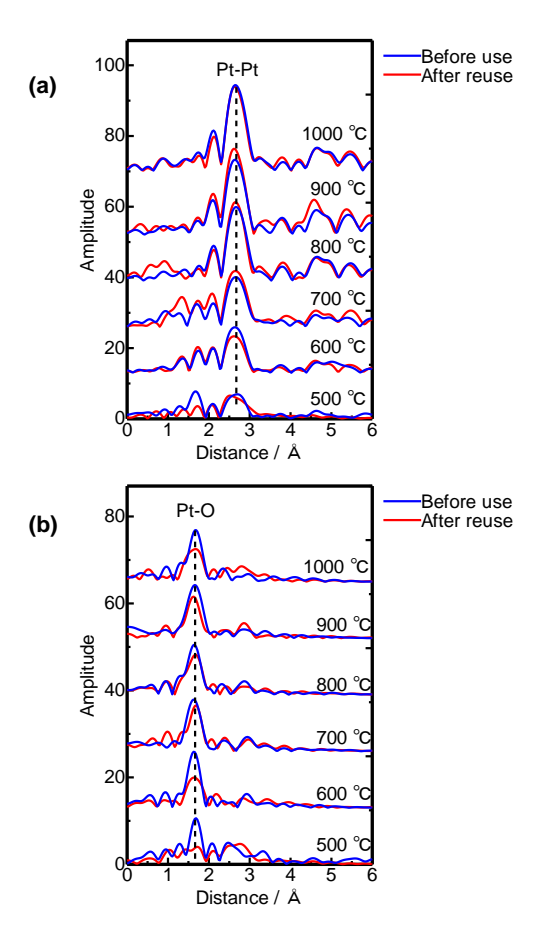


Figure 8. Pt L_3 -edge EXAFS radial distribution function. (a) Pt/ZrO₂ 500-1000C and (b) Pt/CeO₂ 500-1000C before and after the recycling test.

Since hydrosilylation reactions are usually performed under N_2 atmosphere, catalyst recycling tests were conducted in $N_2,\,$ and the results are presented in Figure S9. Interestingly, Pt loaded on ZrO_2 and CeO_2 supports exhibited comparable or even higher reusability in air compared to nitrogen. This suggests that the reoxidation of the catalysts by oxygen in air may play a crucial role in maintaining the high activity of the Pt loaded on ZrO_2 and CeO_2 supports. XAFS measurements were conducted on Pt/CeO_2 and Pt/ZrO_2 catalysts after heat treatment and recycling (Figure 8). For Pt/ZrO_2 , the Pt-Pt coordination peak was prominent following heat treatment, with its intensity increasing at higher

treatment temperature, indicating progressive agglomeration (Figure 8(a)). In contrast, Pt/CeO₂ exhibited a dominant Pt-O peak even after heat treatment, with no detectable Pt-Pt peak at higher temperatures, indicating that Pt remains well-dispersed on the CeO₂ support under these conditions (Figure 8(b)). Comparing the catalysts before and after recycling, Pt/ZrO2 showed no change or an increase in the Pt-Pt peak after recycling (except for the 600 °C heat treatment), implying further Pt agglomeration during the reaction. Figure S10 and S11 present Pt-L₃ edge EXAFS radial distribution functions and XANES spectra before and after recycling in air and N2 atmosphere for highly active catalysts, respectively. A common characteristic of the ZrO₂ and CeO2 supports that showed relatively high activity is that they have basic character. However, if the basicity is too strong, as in the case of MgO, Pt forms a solid solution with MgO.¹⁸ Similar solid solution formation has been observed in Pt-TiO₂ calcined at 900 and 1000 °C.19

The Pt⁴⁺ fraction, derived from XANES analysis (Figure 9), reveals that Pt aggregation occurred to form Pt(0) in all catalysts except Pt/CeO₂ treated at 600 °C. Notably, the Pt/CeO₂ 600C catalyst retained a Pt⁴⁺ content exceeding 70% after recycling, indicating that Pt remains predominantly in a dispersed, oxidized state rather than aggregating into zero-valent Pt particles. This exceptional stability suggests that Pt/CeO₂ 600C maintains its oxidation state and prevents the formation of large Pt clusters, contributing to its sustained catalytic performance.

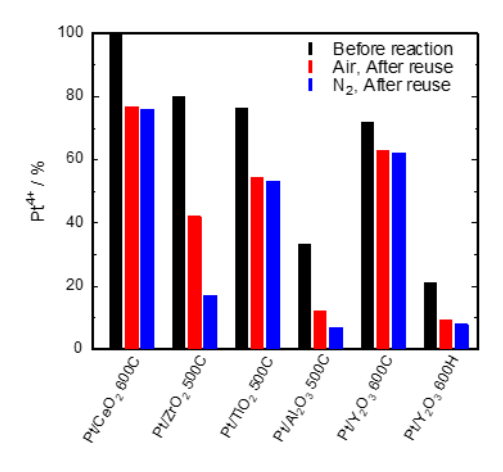


Figure 9. Pt⁴⁺ fraction determined from Pt-L₃ edge XANES before and after recycling in Air and N₂ atmospheres of active catalysts.

Figure 10 presents the expanded XRD pattern focusing on the Pt(111) peak for Pt/ZrO2 and Pt/CeO2. The unenlarged XRD is given in Figure S12. In the XRD of Pt/ZrO2, distinct Pt diffraction peaks are observed at heat treatment temperatures ranging from 800 to 1000 °C, indicating Pt agglomeration at these high temperatures. In contrast, Pt/CeO₂ exhibits no detectable Pt peaks across all treatment temperatures, suggesting that Pt remains highly dispersed on the CeO₂ support, even at elevated temperatures. These results further reinforce the contrasting thermal ability of Pt on ZrO₂ and CeO₂. While high-temperature treatment promotes Pt/ZrO₂, leading to loss of active surface area, Pt/CeO₂ effectively prevents agglomeration, maintaining a finely This enhanced dispersion dispersed Pt state. likely contributes to the superior catalytic performance and durability of Pt/CeO2 in the reaction.

Figure 11(a) illustrates the relationship between the Pt⁴⁺ fraction (from XANES analysis) and the reaction yield for Pt/CeO₂ catalyst as function of the thermal treatment temperature. The data reveals a similar trend, indicating that the presence of Pt in a higher oxidation state (Pt⁴⁺) is associated with enhanced catalytic activity. Figure 11(b) further supports this trend, demonstrating a consistent

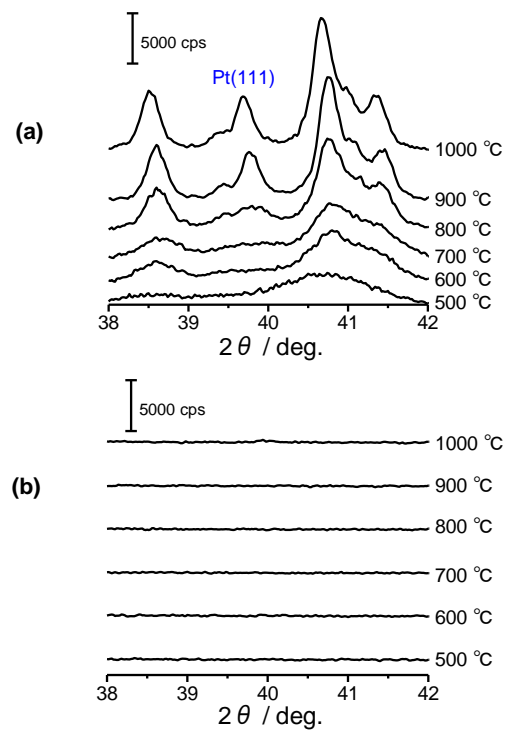


Figure 10. XRD patterns of (a) Pt/ZrO₂ 500-1000C and (b) Pt/CeO₂ 500 – 1000C treated at different temperatures.

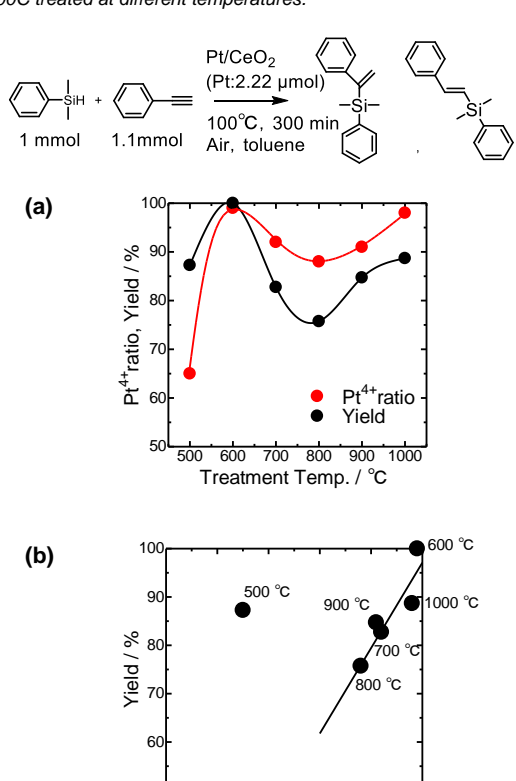


Figure 11. (a) Dependence of Pt^{4+} fraction and yield on thermal treatment temperature in Pt/CeO_2 500 – 1000C. (b) Correlation between Pt^{4+} fraction and yield of Pt/CeO_2 500 – 1000C.

70 80 90 Pt⁴⁺ratio / %

60

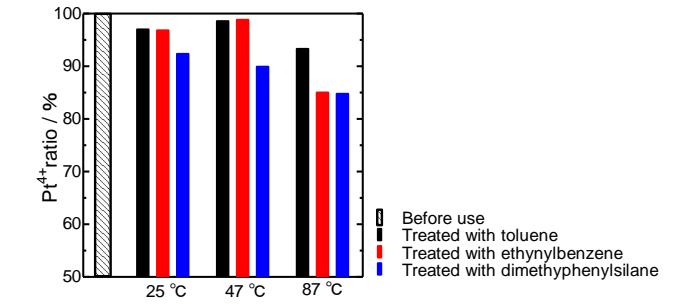


Figure 12. Pt⁺⁺ fraction determined from XANES in Pt/CeO₂ 600C pretreated with substrate and solvent.

relationship between the Pt⁴⁺ fraction and yield for Pt/CeO₂ catalysts. An exception is observed for Pt/CeO₂ 500C, where catalytic performance deviates from the expected trend. STEM-HAADF analysis confirms significant Pt agglomeration in this catalyst as displayed in Figure S3, suggesting that the loss of dispersion diminishes the number of accessible active sites, thereby reducing the overall activity. These findings highlight the crucial role of Pt dispersion and oxidation state in maintaining high catalytic efficiency, with Pt/CeO₂ effectively stabilizing Pt⁴⁺ species and sustaining superior reactivity.

Figure S13(a) and (b) show the N₂ adsorption isotherms of Pt/CeO₂ catalysts and the relationship between the specific surface area and heat treatment temperature for Pt/supports, respectively. As the heat treatment temperature increased, the specific surface area of Pt/CeO2 decreased, with a notable reduction observed between 600 and 700 °C. This reduction in surface area at higher temperatures may contribute to the observed catalytic behavior of Pt/CeO₂. The superior activity of Pt/CeO2 treated at 600 °C can be attributed, in part, to the retention of sufficient surface area to maintain a high density of accessible active sites. Above 700 °C, further decreases in surface area likely led to reduced exposure of active Pt species, diminishing catalytic performance. The significant decrease in activity when reusing Pt catalysts with TiO2, Y2O3, Nb2O5, and La2O3 supports may be due to their low surface area.

To confirm whether Pt^{4+} dispersed on the surface of Pt/CeO_2 600C is reduced by the reactants and solvent (toluene) after heat treatment, XAFS measurements were conducted on Pt/CeO_2 600C pretreated with the reactants, and the Pt^{4+} fraction was determined from XANES analysis. The treatment involved stirring the catalyst at 25, 47 and 87 °C for 3 h at 600 rpm in either 5 mL of toluene solvent or a solution containing 1 mmol of ethynylbenzene and 1 mmol of dimethylphenylsilane in 5 ml of toluene. The results at 87 °C (Figure 12) revealed that Pt^{4+} is reduced to Pt(0) in the presence of the reactants, as evidenced by 8% increase in Pt(0) when dimethylphenylsilane and ethynylbenzene were used compared to toluene alone. This suggests that the reactants actively participate in the reduction of Pt^{4+} to Pt(0) during the reaction.

The H_2 -temperature-programmed reduction (H_2 -TPR) profile of CeO_2 and Pt/CeO_2 catalysts heat-treated at various temperatures is shown in Figure 13. A progressive decrease in the reduction peak intensity was observed in the H_2 -TPR curves of CeO_2 with increasing heat treatment temperature, which may be attributed to sintering of CeO_2 . In Pt/CeO_2 , it has been reported that the peaks observed up to 350 °C correspond to the reduction of oxygen species adsorbed on the surface, as well as Pt-O-Pt and Pt-O-Ce interactions. For Pt/CeO_2 500C the exposed surface CeO_2 contributes to these reduction peaks. However, in Pt/CeO_2 catalysts heat-treated between 600 and 800 °C, these peaks disappeared, suggesting that the surface CeO_2 becomes covered by dispersed Pt particles, which alters the reduction behavior.

This indicates that the dispersion of Pt on the surface plays a critical role in influencing the reducibility and surface properties of Pt/CeO₂ catalysts.

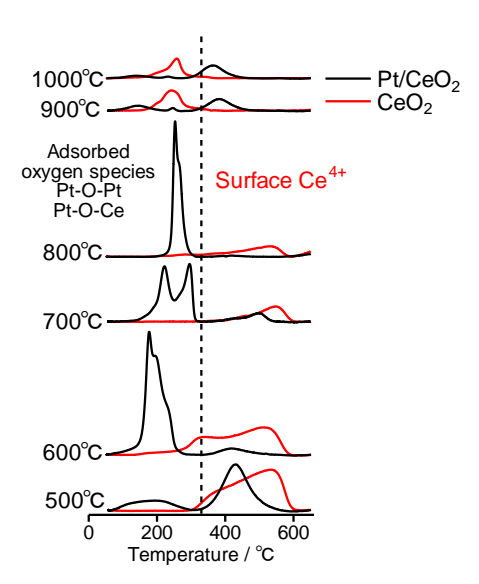


Figure 13. H₂-TPR curves of CeO₂ and Pt/CeO₂ heat-treated at various temperatures.

Figure 14 illustrates that Pt/CeO₂ 600C exhibited the highest catalytic activity in the alkyne reaction. This high activity is attributed to the Pt⁴⁺ species dispersed on the surface after heat treatment at 600°C, which are partially reduced to Pt(0) by the substrate, potentially forming high active single-site catalytic centers. This transformation likely enhances catalytic efficiency by facilitating optimal metal-support interactions and electronic modifications, thereby improving the overall reaction performance.

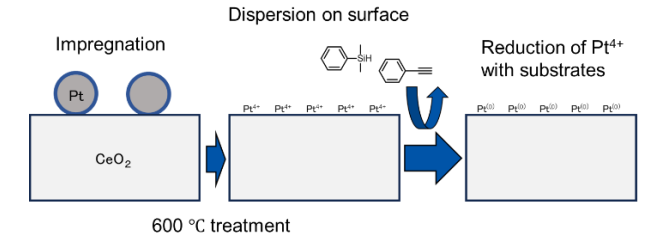


Figure 14. Proposed mechanism for the formation of high activity of Pt/CeO_2 600C in reaction with alkyne.

Detailed characterization of all reaction products and the NMR data are given in the Supporting Information.

Conclusion

In this study, we aimed to develop heterogeneous catalysts as viable alternatives to homogeneous systems for the hydrosilylation of alkenes and alkynes. The choice of support and thermal treatment can significantly influence the structure, electronic properties, and catalytic behavior of supported Pt catalysts. To explore these effects, we prepared Pt catalysts on nine distinct metal oxide supports via impregnation and heat treatment, evaluating their performance in alkene and alkyne hydrosilylation. Among the tested catalysts, Pt/CeO₂ 900H, prepared by supporting Pt on CeO₂, heat-treated at 900 °C, and reduced at 500 °C under a hydrogen stream, demonstrated the highest activity for alkene hydrosilylation. Its performance was comparable to the industrially used Karstedt catalyst, achieving a maximum turnover number (TON) of 6.9 \times 10 6 . Notably, all catalysts exhibited TONs exceeding 5.3 x 104 across various substrates. Characterization of Pt/CeO2 900H revealed that Pt, initially dispersed or dissolved within the CeO₂ matrix during heat treatment, was deposited as Pt nanoparticles

upon reduction, contributing to its exceptional catalytic activity. For alkyne hydrosilylation, Pt/ZrO₂ 500C and Pt/CeO₂ 600C exhibited high activity and were successfully reused for up to 10 cycles particularly in Pt/CeO2 600C. A correlation was observed between reaction yield and the proportion of Pt4+ species, as determined by Pt L3-edge XANES analysis at different heat treatment temperatures. Post-reaction XAFS measurements indicated that Pt was partially reduced during the reaction, suggesting that single-site Pt(0) species, generated in situ, plays a key role in catalytic activity and reusability. These findings highlight the critical role of support selection and thermal treatment in controlling Pt dispersion and oxidation states, enabling the design of highly active and heterogeneous catalysts for hydrosilylation reusable reactions.

Experimental Section

Catalyst preparation: Pt was loaded on nine metal oxide supports (MgO, Al₂O₃, SiO₂, TiO₂, Y₂O₃, ZrO₂, Nb₂O₅, La₂O₃, and CeO₂) by an impregnation method of Pt nanoparticles solution precursors (Renaissance Energy Research) on the supports. The list of oxides used as Pt support is shown in Table 7. The Pt nanoparticle solution was mixed with 100 mL of solvent (H_2O : EtOH = 9: 1) and 2 g of metal oxide support. The Pt loading of was 0.7 wt%. The solvent was then removed using a rotary evaporator. The resulting powder was ground in an agate mortar and heat-treated in air at temperatures ranging from 500 to 1000 °C, with a heating rate of 10 K min⁻¹ and a holding time of 3 h. After natural cooling, the heat-treated samples were crushed in an agate mortar. Finally, the catalysts were obtained by reducing the heat-treated powder in a hydrogen gas flow at 500 °C. The prepared catalyst was used for the hydrosilylation reaction in the liquid phase.

Table 7. List of Oxides used as the support for Pt

Oxide Support	Sample Name	Source
MgO	500A	Ube Material Industries Co.
Al_2O_3	JRC-ALO-6	Reference Catalyst, Catalysis Society of Japan
SiO ₂	CARiACT- Q10	Fuji Silysia Co.
TiO ₂	P90	Evonik Co.
Y_2O_3	250-00442	Fujifilm-Wako Pure Chemical Co.
ZrO_2	JRC-ZRO-9	Reference Catalyst, Catalysis Society of Japan
Nb_2O_5	HY-340	CBMM
La_2O_3	La ₂ O ₃	Prepared according to the literature ²¹
CeO ₂	JRC-CEO-6	Reference Catalyst, Catalysis Society of Japan

Catalytic reaction and analysis: Alkenes, alkynes, and hydrosilanes were purchased from Tokyo Chemical Industry Co. Hydrosilylation reactions were performed using the prepared catalysts. The reaction mixture, comprising alkene or alkyne, silane, and tridecane as an internal standard, was added to a pressure-resistant tube along with a 4 x 10 mm stirrer. The tube was then heated to a predetermined temperature while stirring at 600 rpm. Product analysis was conducted using GC-FID or ¹H NMR. For GC-FID, 2-3 drops of the reaction solution were periodically sampled, diluted with acetone, and analyzed with GC-FID (Shimadzu Co, GC-2025) equipped with a capillary column (GL Science Co, InertCap 1). The yield was calculated by the internal standard method using tridecane as the internal standard. For NMR. the sample was diluted with chloroform-d₁, spiked with 3,4,5trichloropyridine as an internal standard, and analyzed accordingly. ¹H (400 MHz) and ¹³C (100 MHz) NMR spectra were recorded on a JEOL ECZ-500 spectrometer (JEOL) in CDCl₃ using tetramethylsilane (TMS) as an internal reference standard. High resolution mass spectra (HRMS) obtained with a JEOL JMS-GC MATEII GC-MS system.

For recycle use, the catalyst was recovered by cooling the reaction mixture on ice, centrifuging, and carefully removing the supernatant without disturbing the catalyst. The test tubes containing the catalyst were flushed with N2 gas and stored. The reaction was then repeated under a continuous N2 flow at a rate of 10 mL min⁻¹.

Catalyst characterization: X-ray diffraction (XRD) patterns were acquired under ambient conditions using a MiniFlex Xray diffractometer (Rigaku Co.). The measurements were performed in the 2θ range of 20 to 90° (10 deg. min⁻¹) with Cu Kα radiation. N₂ adsorption/desorption isotherms were measured using a BELSORP mini-X instrument (Microtrac Bel Co.). Prior to analysis, the samples were degassed at 300 °C. XAFS measurements were performed to investigate the local structure of supported Pt species. Measurements were performed at KEK-PF (High Energy Accelerator Research Organization Photon BL-9A Factory) and (spectroscopic crystal: Si(111)) with a proposal number: 2024G563 using the fluorescence method. Approximately 50 mg of the sample was formed into 7.0 mm-diameter pellets for measurement. The X-ray fluorescence was detected with a 7-element silicon drift detector at 298 K in a step-scan mode. The data obtained were analyzed using REX2000 (Rigaku Co.). A Talos F200X G2 microscope (Thermo Fisher Scientific Co.) equipped with an EDX analyzer (Super-X) was used to take STEM-HAADF images of the Pt/CeO2 samples, which was operated at 200 kV. In situ CO adsorption FT-IR measurements were conducted using a IRSpirit spectrometer (Shimadzu Co.) to investigate the CO adsorption characteristics of the samples. The experimental procedure was as follows: First, the empty cell was evacuated to a vacuum for background measurement. The sample was then introduced into the cell, heated to 400 °C, and subjected to hydrogen reduction at 100 Torr for 10 min. Afterward, the sample was evacuated again and cooled to below 40 °C in a vacuum before the first measurement. Subsequently, 10% CO/He was introduced at 100 Torr for the second measurement. Finally, the cell was evacuated to create a vacuum, and a third measurement was performed. H2-TPR measurements were conducted to investigate the reduction characteristics of the samples using BELCAT II (Microtrac Bell Inc.). Samples (0.2-0.5 g) were pretreated in an N₂ gas flow for 15 min, followed by heating from 100 °C to 650 °C at 10 K min^{-1} under an 5%-H₂/Ar flow. Following the H₂-TPR analysis, Pt dispersion was evaluated using CO pulse adsorption. The Pt/CO ratio was assumed to be 1 for the dispersion measurement. For this analysis, samples were reduced at 500 °C for 30 min under hydrogen flow as pretreatment.

Supporting Information

Detailed Characterization of all reaction products and the NMR data are given in the Supporting Information.

Author Contribution Declaration

Declare the author contribution in brief here. e.g., 1st, 2nd 3rd authors design the article, conceived the and review/research plan and experimental strategy. 4th author synthesized the molecules, prepared draft manuscript. Last author confirmed the manuscript preparation and assist in daily laboratory supervision, design the research, analyzed the results, wrote manuscript.

Data Availability Declaration

The authors declare that the data supporting the findings are available within the article and its Supplementary Information file.

Notes

The authors declare no competing financial interest.

Acknowledgements

This research was supported by the Ministry of Education, Science, Sports and Culture, Grant-in-Aid for Scientific Research (C), 22K04833, 2022 - 2024 and 25K08389, 2025 - 2028. Technical support for STEM-HAADF imaging and EDS mapping was supported by Dr. K. Hiraga (Nissan-arc. Co.).

References

- B. Marciniec. Catalysis by transition metal complexes of alkene silylation–recent progress mechanistic implications. *Coord. Chem. Rev.*, **2005**, 249, 2374. https://doi.org/10.1016/j.ccr.2005.02.025
 L. H. Sommer, E. W. Pietrusza, F. C. Whitmore. Peroxide-Catalyzed Addition of Trichlorosilane to 1-Octene. *J. Am. Chem. Soc.*, **1947**, 69,
- Addition of Inchlorosilane to 1-Octene. J. Am. Chem. Soc., 1947, 69, 188. https://doi.org/doi:10.1021/ja01193a508
 Z. T. Ball, 10.17 C-E Bond Formation through Hydrosilylation of Alkynes and Related Reactions, Comprehensive Organometallic Chemistry III, Vol. 10 (Eds.: D. M. P. Mingos, R. H. Crabtree). Elsevier Science, 2007, 789-813. https://doi.org/10.1016/B0-08-045047.4/001204
- G. Pan, C. Hu, S. Hong, H. Li, D. Yu, C. Cui, Q. Li, N. Liang, Y. Jiang, L. Zheng, L. Jiang. Biomimetic caged platinum catalyst for hydrosilylation reaction with high site selectivity. *Nat. Commun.*,
- hydrosilylation reaction with high site selectivity. *Nat. Commun.*, **2021**, *12*, 64. https://doi.org/10.1038/s41467-020-20233-w
 L. D. de Almeida, H. Wang, K. Junge, X. Cui, M. Beller. Recent Advances in Catalytic Hydrosilylations: Developments beyond Traditional Platinum Catalysts. *Angew. Chem. Int. Ed. Engl.*, **2021**, *60*, 550. https://doi.org/10.1002/anie.202008729
 K. Kamata, A. Suzuki, Y. Nakai, H. Nakazawa. Catalytic hydrosilylation of alkenes by iron complexes containing terpyridine derivatives as ancillary ligs. *Organometallics*, **2012**, *31*, 3825. https://pubs.acs.org/doi/10.1021/om300279t
 L. K. Goncharova, R. A. Novikov, I. P. Beletskaya, A. V. Arzumanyan. Recyclable convenient-to-hle Pt/ethylene glycol catalytic system an approach to sustainable hydrosilylation. *J. Catal.*, **2023**, *418*, 70. https://doi.org/10.1016/j.jcat.2023.01.004
- approach to sustainable hydrosilylation. *J. Catal.*, **2023**, *418*, 70. https://doi.org/10.1016/j.jcat.2023.01.004
 T. K. Meister, K. Riener, P. Gigler, J. Stohrer, W. A. Herrmann, F. E. Kühn. Platinum Catalysis Revisited—Unraveling Principles of Catalytic Olefin Hydrosilylation. *ACS Catal.*, **2016**, *6*, 1274. https://doi.org/10.1021/acscatal.5b02624
 L. W. Chung, Y.-D. Wu, B. M. Trost, Z. T. Ball. A Theoretical Study on the Mechanism, Regiochemistry, and Stereochemistry of Hydrosilylation Catalyzed by Cationic Ruthenium Complexes. *J. Am. Chem. Soc.*, **2003**, *125*, 11578. https://doi.org/10.1021/ja034833

- J. Heveling. Heterogeneous catalytic chemistry by example of industrial applications. *J. Chem. Edu.*, **2012**, *89*, 1530. https://doi.org/10.1021/ed200816g
 Y. Watanabe, Catalysis of Pt Clusters on Metal Oxide, in Encyclopedia of Interfacial Chemistry, K. Welt Ed. Oxford: Elsevier, **2018**, 398-405. https://doi.org/10.1016/B978-0-12-409547-2-12983-X
- T. W. veelen, C. Hernández Mejía, K. P. de Jong. Control of metal-support interactions in heterogeneous catalysts to enhance activity selectivity. *Nat. Catal.*, **2019**, *2*, 955. <a href="https://doi.org/10.1038/s41929-
- 019-0364-x Y. Nakajima, S. Shimada. Hydrosilylation reaction of olefins: recent advances perspectives. *RSC Adv.*, **2015**, *5*, 20603.
- advances perspectives. *RSC Adv.*, **2015**, 5, 20603. https://doi.org/10.1039/c4ra17281g
 L. Zhang, M. Zhou, A. Wang, T. Zhang. Selective Hydrogenation over Supported Metal Catalysts: From Nanoparticles to Single Atoms. *Chem. Rev.*, **2020**, *120*, 683.
- https://doi.org/10.1021/acs.chemrev.9b00230
 X. Cui, K. Junge, X. Dai, C. Kreyenschulte, M. M. Pohl, S. Wohlrab, F. Shi, A. Bru ckner, M. Beller. Synthesis of Single Atom Based Heterogeneous Platinum Catalysts: High Selectivity Activity for Hydrosilylation Reactions. ACS Cent. Sci., 2017, 3, 580.
- Heterogeneous Platinum Catalysts: High Selectivity Activity for Hydrosilylation Reactions. ACS Cent. Sci. 2017, 3, 580. https://doi.org/10.1021/acscentsci.7b00105
 Y. Chen, S. Ji, W. Sun, W. Chen, J. Dong, J. Wen, J. Zhang, Z. Li, L. Zheng, C. Chen, Q. Peng, D. Wang, Y. Li. Discovering Partially Charged Single-Atom Pt for Enhanced Anti-Markovnikov Alkene Hydrosilylation. J. Am. Chem. Soc., 2018, 140, 7407. https://doi.org/10.1021/jacs.8b03121
 C. J. Kong, S. E. Gillil, B. R. Clark, B. F. Gupton. Highly-active, graphene-supported platinum catalyst for the solventless hydrosilylation of olefins. Chem. Commun., 2018, 54, 13343. https://doi.org/10.1039/c8cc07641c
 K. Okumura, H. Hoshi, H. liyoshi, H. Takaba. Formation of a Pt-MgO Solid Solution: Analysis by X-ray Absorption Fine Structure Spectroscopy, ACS Omega, 2022, 7, 27458. https://doi.org/10.1021/acsomega.2c02486
 M. Hatanaka, N. Takahashi, T. Tanabe, Y. Nagai, K. Dohmae, Y. Aoki, T. Yoshida H. Shinjoh. Ideal Pt loading for a Pt/CeO₂-based catalyst stabilized by a Pt-O-Ce bond. Appl. Catal. B, 2010, 99, 336. https://doi.org/10.1016/j.apcatb.2010.07.003
 K. Okumura, R. Chihara, A. Abdullahi, M. Kato. Characterization of the active species in the aerobic oxidation of benzyl alcoholestell/2016 by Pt/Crop. Mol. Cotol. B, 2026, 572, 11480.

- K. Okumura, R. Chinara, A. Abdullahi, M. Kato. Characterization of the active species in the aerobic oxidation of benzyl alcohol catalyzed by Ru/ZrO₂. *Mol. Catal. B*, **2025**, *573*, 114820. https://doi.org/10.1016/j.mcat.2025.114820
 H. Chuanqing, Y. Yingzhi, Y. Yue, W. Dashan, H. Feiyang, W. Xuewen, Z. Rongbin, F. Gang, Y. Jinmei. Ru/La₂O₃ catalyst for ammonia decomposition to hydrogen. *Appl. Surf. Sci.*, **2019**, *476*, 928. https://doi.org/10.1016/j.apsusc.2019.01.112